Stress Measurement of SS400 Steel Beam Using the Continuous Indentation Technique

by Y.-H. Lee, W.-j. Ji and D. Kwon

ABSTRACT—An analytical model is presented for determining surface residual stress using continuous indentation. The elastic residual stress is assumed to have no influence on contact area or hardness and to be uniform over a volume that is several times larger than the indentation mark. A step-by-step analysis for the residual-stress-induced load difference at a given depth is outlined here and such concepts as stress interaction, stress-sensitive contact morphology, and reversible contact recoveries during a stress relaxation are described. Finally, the proposed method is applied to the interpretation of the continuous indentation results obtained from an SS400 steel beam in which controlled bending stresses are generated. The stress estimated, however, showed a high scatter due to plastic pile-up deformation. When the optically measured contact area is used as an alternative of the contact area calculated from the unloading curve, the re-evaluated stress agrees well with the already known applied stress.

KEY WORDS—Residual stress, continuous indentation, stress interaction, stress relaxation

Introduction

A number of lab-scale stress-measurement techniques have been developed over the last few decades.[1] In general, a distinction is made between destructive and non-destructive techniques. Destructive methods, including hole drilling and saw cutting, measure the relaxation strain directly by removing part of the stressed structure.[1,2] These techniques are sensitive to the macroscopic residual stress and measure the stress quantitatively without any information on the unstressed reference state. However, they have limited industrial applications because they are destructive and because the removal of material may create additional stress. Among the non-destructive methods are the neutron and x-ray diffractions, magnetic Barkhausen noise, and ultrasonic method,[1,2] all based on the relationship between physical or crystallographic parameters and residual stress. Recently, the neutron diffraction method, with its deep penetration capacity, has been highlighted because it can measure residual strains throughout the thickness of a structure. However, it is infrequently used in the laboratory because neutron sources are rare and costly. X-ray diffraction has been used in numerous previous studies, but measures only near surface strain due to its shallow penetration capacity. The results of the magnetic Barkhausen noise and the ultrasonic methods are measured by empirical calibration rather than a theoretical stress analysis, and are thus useful only for comparative assessments. In addition, the results of non-destructive techniques show low reproducibility and high scatter because they are very sensitive to metallurgical factors including microphase, grain size, and texture and to such environmental factors as external vibration, electric, and magnetic fields.

An almost non-destructive continuous indentation technique has recently been developed to characterize such mechanical properties as hardness, elastic modulus,[3] and true stress–strain relation[4] from an indentation load versus depth curve representing the elastic/plastic deformation response beneath a rigid indenter. The first analysis step on the raw indentation curve is to calculate from the unloading curve contact properties such as initial unloading slope or contact stiffness, contact depth, and contact area. The contact depth h_C was determined, using Oliver and Pharr's analysis,[3] from the power-law fitted unloading curve in Fig. 1. S and h_i are, respectively, the contact stiffness and intercept depth of the tangent to the unloading curve, and the contact area A_C is expressed as $24.5h_C^2$ for a Vickers pyramid with an apex angle 136°. The indenter used here was observed through an atomic force microscope and a line defect less than 1 μm long was found at the apex. Thus, the self-similarity of the Vickers geometry was approximated for the whole indenter.

In this study, the continuous indentation technique was applied to character a simple stress state in a steel beam. Figure 1 compares the dotted indentation loading curves corresponding to the compressive and tensile stresses with the solid indentation curve of the unstressed state.[5,6] The indentation load L_0 for the unstressed state decreases to L_T due to the tensile residual stress, while L_0 increases to L_C because of the compressive residual stress at a same depth h_t.[7] This stress-induced load difference is explained through a stress-sensitive contact morphology and an interaction between the indentation stress and the residual stress. Reversible recovery responses in the load and contact morphology were also described during continuous stress relaxation. Finally, an equation for a simple uniaxial residual stress is proposed and verified through continuous indentation tests on a stressed sample.

Theoretical Model

Definition of a Residual-Stress-Induced Normal Load for Uniaxial Residual Stress

The stress state in a plastic core beneath an indenter is considered as a hydrostatic stress in the first term of eq (1).[8,9] The

Y.-H. Lee (uni44@mmrl.snu.ac.kr) is a Post-doctoral Researcher, W.-j. Ji is a Graduate Student and D. Kwon is a Professor, School of Materials Science and Engineering, Seoul National University, Seoul 151-742, Korea.

Original manuscript submitted: July 27, 2002.
Final manuscript received: May 24, 2003.
DOI: 10.1177/0014485104039750

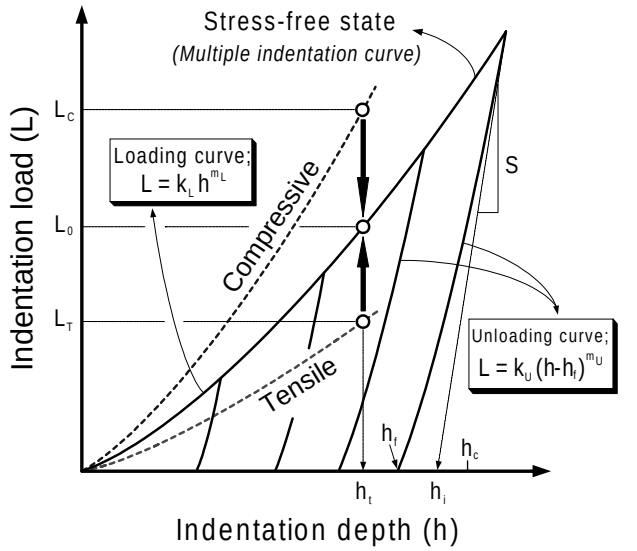

Fig. 1—Schematic diagram of the theoretical analysis of indentation unloading curve[3] and change in indentation loading curves by the effect of stress states[5–7,10]

diagonal quantity of the hydrostatic stress is $-2\sigma_{ys}/3$, where σ_{ys} is yield strength. A uniaxial residual stress has only the stress component of σ_{xx}. The influence of the uniaxial residual stress on indentation plasticity is analyzed as follows. From the point of view of the shear plasticity, the combined stress σ_{com}, composed of the above-mentioned indentation and uniaxial residual stresses, is separated into two parts, a hydrostatic stress (mean stress) and a plastic deformation-sensitive deviator stress:

hydrostatic stress in core — uniaxial residual stress

$$\sigma_{com} = \begin{pmatrix} -\frac{2}{3}\sigma_{ys} & 0 & 0 \\ 0 & -\frac{2}{3}\sigma_{ys} & 0 \\ 0 & 0 & -\frac{2}{3}\sigma_{ys} \end{pmatrix} + \begin{pmatrix} \sigma_{res} & 0 & 0 \\ 0 & 0 & 0 \\ 0 & 0 & 0 \end{pmatrix}$$

separated hydrostatic stress σ^H

$$= \begin{pmatrix} -\frac{1}{3}(2\sigma_{ys} - \sigma_{res}) & 0 & 0 \\ 0 & -\frac{1}{3}(2\sigma_{ys} - \sigma_{res}) & 0 \\ 0 & 0 & -\frac{1}{3}(2\sigma_{ys} - \sigma_{res}) \end{pmatrix}$$

deformation-sensitive deviator stress σ^D

$$+ \begin{pmatrix} \frac{2}{3}\sigma_{res} & 0 & 0 \\ 0 & -\frac{1}{3}\sigma_{res} & 0 \\ 0 & 0 & -\frac{1}{3}\sigma_{res} \end{pmatrix}. \quad (1)$$

The stress component parallel to the indentation axis (the z-axis) in the deviator stress part, $\sigma^D_{zz} = -\sigma_{res}/3$, adds directly to the surface-normal indentation pressure. Thus, the contribution of the residual stress to the total indentation load is defined as a residual-stress-induced normal load L_{res} in eq (2) by multiplying the contact area A_C with the deviator stress component σ^D_{zz}; the quantity L_{res} is measured from the load difference between the unaxially stressed and the unstressed samples at the same depth:

$$L_{res} = -\frac{1}{3}\sigma_{res} A_C. \quad (2)$$

Residual-Stress-Induced Change in the Contact Area

Previous indentation studies[5–7,10] on artificially stressed states report two significant experimental and simulation results. The first is the increment or decrement in the indentation load due to compressive or tensile residual stresses at a given depth, as illustrated in Fig. 1. The second is a stress-independent hardness or contact area,[6,10] identified by close observation of indentation marks[6] and finite element simulation of the contact deformations of stressed samples.[10] An indentation contact morphology on a pre-existing tensile stress is modeled in Fig. 2 based on two aforementioned facts as premises. In order simultaneously to satisfy the lower indentation load L_T and the stress-independent hardness H expressed in eq (3), the contact area A_C^T and the contact depth h_C^T in the tensile-stressed sample must be smaller than in the unstressed sample:

$$H = \frac{L_T}{A_C^T} = \frac{L_0}{A_C} = \frac{L_C}{A_C^C}. \quad (3)$$

This means that a significant contact feature under tensile stress is sink-in deformation h_n or smaller pile-up deformation than in the unstressed state, as illustrated in Fig. 2,[7] although larger contact area A_C^C and indentation load L_C in the compressive-stressed sample are predicted by similar arguments. If the tensile residual stress (solid arrows) is removed at the constant depth h_t, the indentation load and contact morphology in Figs. 1 and 2 will return to those of the unstressed state by a reversible recovery. Thus, the final equation for the residual stress is derived from the fundamental equation (2) with detailed information on the indentation load and contact morphology during the stress relaxation.

A Depth-Controlled Stress-Relaxation Procedure

Figure 2 shows the change in contact morphology during stress relaxation at a given depth h_t constrained by a rigid frame. A rebounding force is generated by the removal of the tensile residual stress (solid arrows) that pushes the indenter out from the sample surface.[7] However, the rebounding force is constrained by the rigid frame to manifest itself as continuous increases in indentation load ($L_T \rightarrow L_0$) and contact area ($A_C^T \rightarrow A_C$). The continuous changes in indenting deformation during the tensile stress relaxation are expressed as an integral equation by inserting the definition of L_{res} into eq (4):

$$L_0 = L_T + L_{res} = L_T - \frac{1}{3}\int_{L_T}^{L_0} d(\sigma \cdot A_C). \quad (4)$$

The behaviors of the contact area A_C and the in-plane stress σ during the stress relaxation must be expressed in term of the indentation load L to solve the integral equation. Linear relaxation of the residual stress is assumed, as in eq (5); the

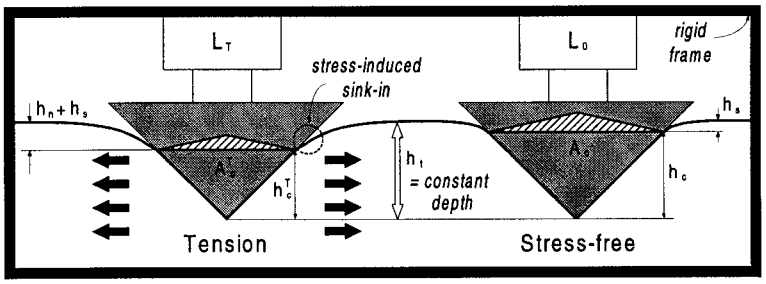

Fig. 2—Contact area under tensile residual stress (solid arrows) increases to large contact area for the unstressed state by elimination of sink-in deformation during depth-controlled stress-relaxation procedure[7]

residual stress of the tensile-stressed state is initially σ_{res} and decreases to zero for the final unstressed state:

$$\sigma = \left(\frac{\sigma_{res}}{L_{res}}\right) L_0 - \left(\frac{\sigma_{res}}{L_{res}}\right) L. \tag{5}$$

The contact area, determined from the unloading curve analysis of the unstressed sample, is also used in expressing its variation during stress relaxation because a unique contact area exists for a given load, according to the premise of the residual stress-independent hardness. The contact area can be expressed as the maximum indentation load divided by hardness, L/H, for a geometrically perfect angled indenter and homogeneous specimen. However, the contact area of an actual Vickers indentation on a mechanically ground steel specimen is fitted in eq (6) as an equation of the second degree in the indentation load; R_0, R_1, and R_2 are fitting constants in the polynomial equation of the contact area:

$$A_C = R_2 L^2 + R_1 L + R_0. \tag{6}$$

Equation (7) for the uniaxial residual stress is derived from eq (4) by substituting A_C and σ from eqs (5) and (6). Thus, the residual stress can be calculated from the stress-induced normal load or load shift in the indentation loading curve and the contact area function analyzed from the unloading curve:

$$\sigma_{res} = 3\frac{L_{res}^2}{R_2 L_T^3 + (R_1 - R_2 L_0) L_T^2 + (R_0 - R_1 L_0) L_T - R_0 L_0}. \tag{7}$$

Experimental Procedures

Design of a Uniaxial Stress-Generating Apparatus and Specimen Preparation

The proposed stress-analysis equation was tested experimentally by continuous indentations on a stressed sample. Various uniaxial stress states ($\sigma_x \neq \sigma_y, \sigma_y = \sigma_z = 0$) were applied to a rectangular beam specimen in a four-point bending apparatus in Fig. 3; the applied stress varies linearly along the specimen thickness from tensile stress near the outer span to compressive stress near the inner span. The SS400 steel specimen was stress-relief heat-treated; Table 1 shows its chemical composition and mechanical properties. A rectangular beam $30 \times 24 \times 200$ mm^3 was annealed at 500°C for 1 h and slowly cooled down to room temperature. The outer and inner spans of the apparatus were 160 and 30 mm, respectively. The elastic bending strain, produced on the specimen by a screw joining the inner and outer dies was measured by strain gages attached to the upper and lower surfaces of the mechanically ground specimen and was converted to the applied stress value by multiplying the Young's modulus of the specimen. The gradient of the bending stress is the same inside the inner span and the continuous indentation tests were performed in this region.

Continuous Indentation Tests on the Uniaxially Applied Stress States

The continuous indentation tests were performed using a AIS 3000R system made by the Frontics, Inc. whose load and depth resolutions were 1.5 gf and 0.1 μm, respectively. A multiple indentation method including loading, unloading and reloading cycles at various load steps was adopted in the unstressed state to analyze the load-dependent function of the contact area by making one residual indentation mark. More than three Vickers indentation tests were performed on the unstressed specimen with indentation load steps 20, 25, 30, 35, and 40 kgf and testing speed 0.3 mm min^{-1}. The contact depth at each indentation load step was analyzed using the analysis of Oliver and Pharr[3] and converted to the contact area. In addition to the multiple indentation tests, single indentation curves from one indentation loading and unloading cycle were also obtained and compared with the shape of multiple curves to confirm that the different indentation procedures do not influence the indentation response. In addition, the indentation marks were optically observed and compared with the theoretically calculated contact areas.

A single indentation curve corresponding to each stress state was obtained from the elastically bent beam specimen. The indentation load and testing speed were 40 kgf and 0.3 mm min^{-1}, respectively. Three indentation arrays were formed along the thickness direction inside the inner span. The space between indentation marks was 3 mm (to avoid superposing the adjacent deformation fields). Indentation curves from the unstressed and stressed states were superposed and analyzed using the model proposed here.

Results and Discussion

Influence of Residual Stress on the Indentation Loading Curve

The single and multiple indentation curves from the unstressed sample superposed perfectly within the depth

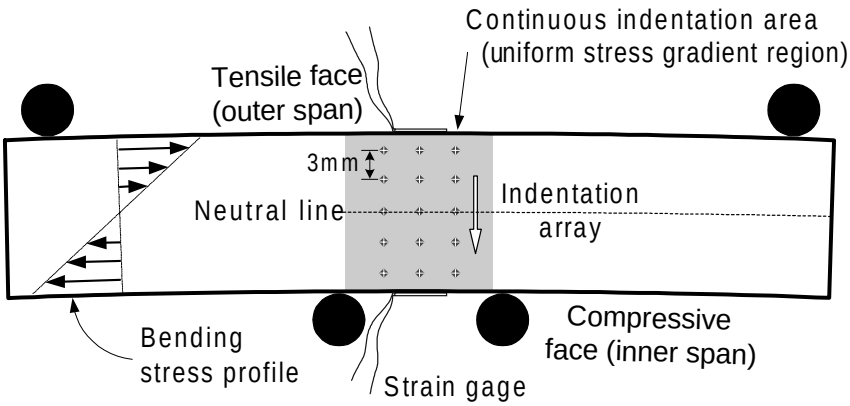

Fig. 3—Indentation arrays at various stresses applied through a four-point bending apparatus

TABLE 1—CHEMICAL COMPOSITION AND MECHANICAL PROPERTIES OF SS400 STEEL

Element *t*	*C*	*Mn*	*Si*	*S*	*P*	*Fe*	Elastic Modulus (GPa)	Poisson's Ratio	Yield Strength (MPa)
wt(%)	0.148	0.458	0.213	0.018	0.012	Bal.	209	0.29	267

deviation range ± 0.3 μm at the maximum indentation load (see Fig. 4 (a)). The contact depths were calculated from the unloading curves corresponding to several load steps and converted to the contact areas using the Vickers pyramidal geometry. The contact areas in Table 2 were fitted as an equation in the indentation load; the fitting constants were –27031.197, 641.884, and 0.075 for R_0, R_1, and R_2, respectively. The indentation loading curves for two applied stresses are superposed on that of the unstressed specimen in Fig. 4 (b). The loading curve for the compressive or tensile applied stress shifted to the left or right of that of the unstressed sample, as might be expected. All indentation loading curves are fitted in a form $L = k_L h^{m_L}$ in Table 3 rather than a quadratic function $L = k_L h^2$ dependent on the indenter geometry, since better fitting was achieved with the power-law function; the exponent m_L was not 2, but was nearer a value of 5/3, as reported in a previous study.[11,12] Among the reasons that the power-law fitting is more suitable are[11] that the work-hardened layers on the surface of steel samples influence the deformation response, there is friction between the indenter and sample surface, and the material under test is not ideally homogeneous. Other deformation processes concerning densification or cracking in ceramics may be involved. Two indentation loads corresponding to the stressed and unstressed samples at the given depth were used as the lower and upper limits in eq (4), and the residual-stress-induced normal load in eq (7) was determined from the load difference. The stress values under four-point bending were evaluated by substituting the analyzed contact area function and L_{res} into the final equation (7); they are compared with the already known uniaxial applied stresses in Fig. 5.

Stress Evaluation Based on the Proposed Indentation Analysis

The stress evaluated from the indentation arrays in Fig. 5 had a trend similar to that of the applied stresses but deviated from them in absolute value. This is explained by an unexpected contact deformation in ductile metal. The indentation tests on SS400 steel were accompanied a severe plastic pile-up deformation around the remnant indentation mark, but the contact area calculated from elastic analysis of the unloading curve cannot take into account the increase in actual contact area occasioned by this plastic pile-up. Thus, the contact area from the analysis of Oliver and Pharr[3] must be compared with the optically measured actual contact area. The large scatter in the tensile-stressed region is considered to be the result of an inhomogeneous and stress-directionality-dependent pile-up deformation in a previous study,[13] whereas a stress-directionality-independent concentric pile-up shape appeared in the compressive-stressed region.

Modification of Contact Area Considering the Pile-Up Deformation

The actual contact area A_C^{Pile}, taking into account the pile-up deformation around the indentation mark, was measured by optical observation in Fig. 6(a) and compared with the theoretically determined contact area A_C. A pile-up correction ratio of A_C^{Pile} to A_C at maximum indentation load was 1.209 and was taken as invariant regardless of the indentation load. The actual contact area for each load step was taken as the product of A_C and the pile-up correction ratio. The cross-sectional shape of the Vickers indentation on SS400 steel is also shown in Fig. 6(b). Thus, the final equation for the residual stress was modified by the pile-up correction ratio because a load-supporting contact area is not the theoretically calculated contact area but the actual area A_C^{Pile} including the pile-up deformation. The actual contact area was refitted as an equation in the indentation load, and the constants determined in eq (6) were –32668.268, 775.742, and 0.090 for R_0, R_1, and R_2, respectively.

The residual stress recalculated according to the modified model agreed well with the measured applied stress within a standard deviation of ± 43.95MPa (see Fig. 7). In particular, the stress in the tensile-stressed region, critical in the

TABLE 2—CONTACT PROPERTIES EVALUATED FROM THE UNLOADING PARTS OF THE MULTIPLE INDENTATION CURVES FOR SS400 STEEL BEAM AT THE UNSTRESSED STATE

Indentation Load (N)	Indentation Depth (μm)	Contact Depth (μm)	Contact Area (μm^2)
196	69.3 $\pm$ 0.3	65.2 $\pm$ 0.3	104204.0 $\pm$ 866.5
245	78.8 $\pm$ 0.1	74.3 $\pm$ 0.1	135080.4 $\pm$ 278.2
294	87.5 $\pm$ 0.1	82.9 $\pm$ 0.2	168512.8 $\pm$ 607.2
343	95.6 $\pm$ 0.1	90.6 $\pm$ 0.4	201279.5 $\pm$ 1699.0
392	103.3 $\pm$ 0.3	97.8 $\pm$ 0.5	234363.1 $\pm$ 2510.8

TABLE 3—POWER-LAW FITTED LOADING CURVES FOR VARIOUS UNIAXIALLY STRESSED AND UNSTRESSED STATES; LOAD DIFFERENCE AT 90 μm IS COMPARED TO APPLIED STRESS

Applied Stress State (MPa)	Fitted Loading Curve	Stress-induced Normal Load at 90μm Indentation Depth (N)
+260.9	$L = 0.1595\ h^{1.6590}$	29.97
+198.2	$L = 0.1188\ h^{1.7345}$	17.11
+115.4	$L = 0.1211\ h^{1.7354}$	0.27
+39.7	$L = 0.1519\ h^{1.6941}$	–2.14
–34.2	$L = 0.1391\ h^{1.7186}$	–9.11
–115.8	$L = 0.1612\ h^{1.6900}$	–15.13
–190.0	$L = 0.1839\ h^{1.6656}$	–22.31
Unstressed (0)	$L = 0.1473\ h^{1.6994}$	—

reliability of real structures, is quite compatible with the uniaxial applied stress. This is very encouraging for the prospective application of this continuous indentation technique to local fragile regions in in-field structures. We expect that the present technique on the stress evaluation of monolithic material will be extended to real welds before long. To this end, such important issues as the formation of stress-free samples corresponding to each microstructural region, rapid microstructural gradients, and complex stress states deviating from uniaxial stress must be incorporated. A previous study[14] of steel welded joints reported that the residual stress could be relaxed by proper post-weld heat treatment (PWHT). Thus, we may expect that the first two issues can be handled by one-to-one comparison of the indentation curves from each microstructural region before and after the stress-relaxation heat treatment. The final problem, stress directionality, is being investigated by using an inhomogeneous pile-up deformation and eccentricity of remnant impression formed by a conical indenter, and the sensitivity of a Knoop indenter according to the direction of principal stress. Although various problems must be settled for further in-field applications, this work shows the potential of the continuous indentation technique as a local stress-measuring technique.

Conclusions

A continuous indentation technique for measuring surface residual stress was proposed based on the concepts of the stress interaction and relaxation and was confirmed by experimental tests on artificially applied stress states. The major conclusions are as follows.

1. The effects of residual stress on indentation plasticity are defined from the deformation-sensitive deviator stress component of the uniaxial residual stress, and the definition was combined with the stress-relaxation concept. The following equation for the uniaxial residual stress is proposed:

$$\sigma_{res} = 3\frac{L_{res}^2}{R_2 L_T^3 + (R_1 - R_2 L_0) L_T^2 + (R_0 - R_1 L_0) L_T - R_0 L_0}.$$

2. A uniaxially applied stress was formed on a SS400 beam using a four-point bending apparatus. The stress-induced shift in the indentation loading curve agreed well with the sign of the applied stress, as expected. However, the stress evaluated in the continuous indentation model had some scatter in the tensile-stressed region.

3. The dominant factor in the scattering in the evaluated stress was identified as the increase in the actual contact area by plastic pile-up around the indentation mark. The actual contact area was corrected by direct optical observation, and the recalculated residual stress based on the modified contact information showed good agreement with the uniaxial applied stress. Although various mechanical and metallurgical issues concerning welded joints are not yet settled, the potential of the continuous indentation technique are identified.

Acknowledgments

This work was supported by a grant from the Asian Office of Aerospace Research and Development/Air Force Office of Scientific Research. Parts of this work were funded by the National Research Laboratory Program of the Korean Ministry of Science and Technology.

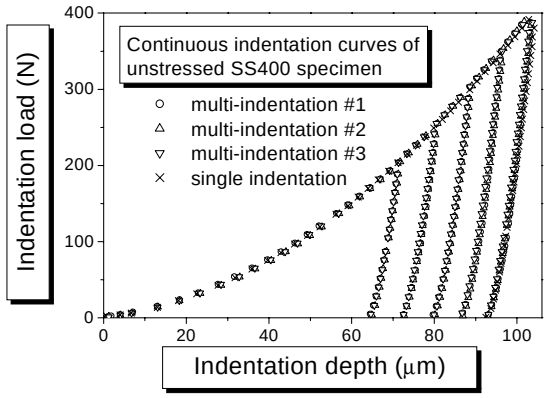

(a)

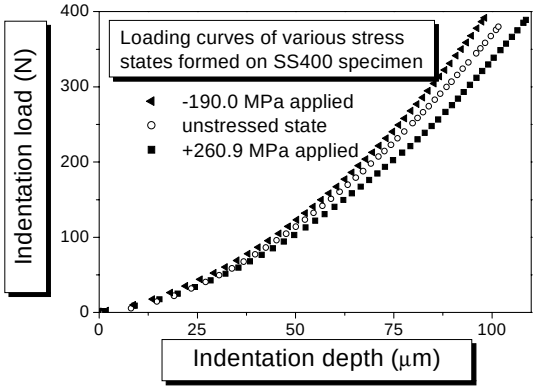

(b)

Fig. 4—Loading deformation and contact properties analyzed from (a) the multiple indentation curves for SS400 in the unstressed state and (b) superposed loading curves from two stress-applied and unstressed states

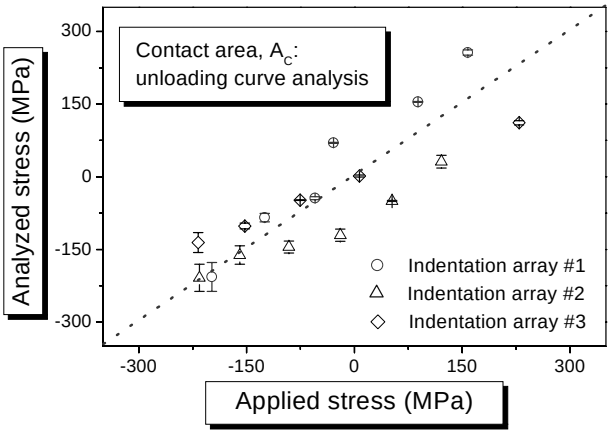

Fig. 5—Stress evaluated by the continuous indentation technique has same trend as already known applied stress but deviates in absolute value. The discrepancy is explained by a plastic pile-up deformation in ductile metal that was not considered in the theoretical contact-area analysis

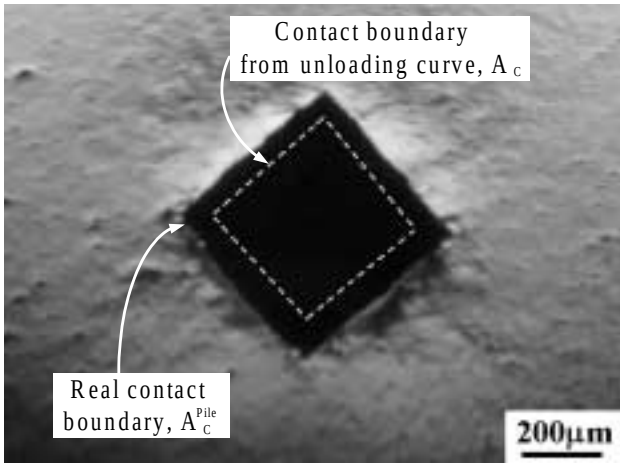

(a)

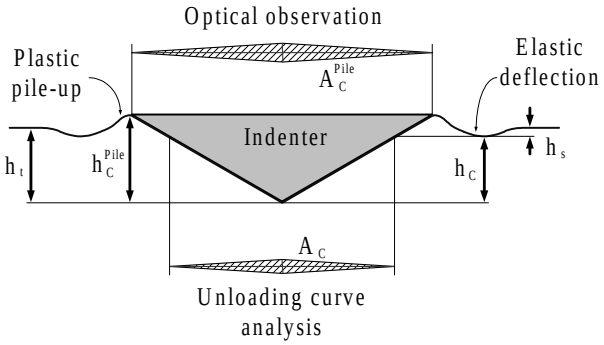

(b)

Fig. 6—Comparison of actual contact area with the theoretically analyzed value: (a) in-plane view of indentation mark and (b) schematic cross-sectional view showing the increase in actual contact area because of plastic pile-up

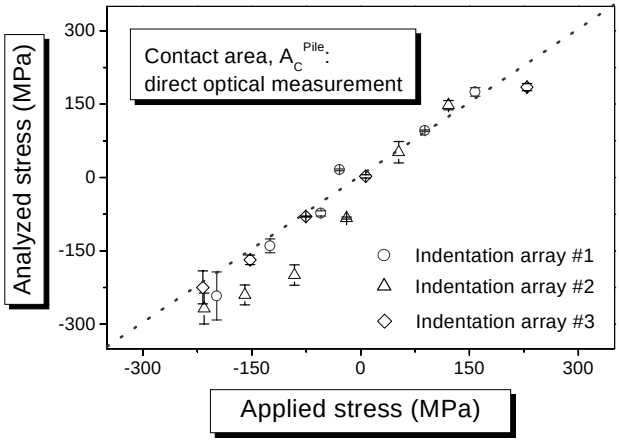

Fig. 7—Stress recalculated using data of the actual contact area agreed well with the already known applied stress

References

1. Lu, J., editor, Society for Experimental Mechanics, Handbook of Measurement of Residual Stresses, Fairmont Press, Lilburn, 228–229 (1996).

2. Ruud, C.O., DiMascio, P.S., and Yavelak, J.J., "Comparison of Three Residual-Stress Measurement Methods on a Mild Steel," EXPERIMENTAL MECHANICS, **25**, 338–343 (1985).

3. Oliver, W.C. and Pharr, G.M., "An Improved Technique for Determining Hardness and Elastic Modulus Using Load and Displacement Sensing Indentation Experiments," Journal of Materials Research, **7** (6), 1564–1583 (1992).

4. Ahn, J.H. and Kwon, D., "Derivation of Plastic Stress–Strain Relationship from Ball Indentation: Examination of Strain Definition and Pileup Effect," Journal of Materials Research, **16** (11), 3170–3178 (2001).

5. LaFontaine, W.R., Paszkiet, C.A., Korhonen, M.A. and Li, C.-Y., "Residual Stress Measurements of Thin Aluminum Metallizations by Continuous Indentation and X-ray Stress Measurement Techniques," Journal of Materials Research, **6** (10), 2084–2090 (1991).

6. Tsui, T.Y., Oliver, W.C., and Pharr, G.M., "Influences of Stress on the Measurement of Mechanical Properties Using Nanoindentation: Part I. Experimental Studies in an Aluminum Alloy," Journal of Materials Research, **11** (3), 752–759 (1996).

7. Lee, Y.-H. and Kwon, D., "Residual Stresses in DLC/Si and Au/Si Systems: Application of a Stress-Relaxation Model to the Nanoindentation Technique," Journal of Materials Research, **17** (4), 901–907 (2002).

8. Johnson, K.L., Contact Mechanics, 1st edition, Cambridge University Press, Cambridge, 171 (1985).

9. Frenkel, J., Abbate, A. and Scholz, W., "The Effect of Residual Stresses on Hardness Measurements," EXPERIMENTAL MECHANICS, **33**, 164–168 (1993).

10. Bolshakov, A., Oliver, W.C. and Pharr, G.M., "Influences of Stress on the Measurement of Mechanical Properties Using Nanoindentation: Part II. Finite Element Simulations," Journal of Materials Research, **11** (3), 760–768 (1996).

11. Mencik, J. and Swain, M.V., "Micro-indentation Tests with Pointed Indenters," Materials Forum, **18**, 277–288 (1994).

12. Hainsworth, S.V., Chandler, H.W., and Page, T.F., "Analysis of Nanoindentation Load-Displacement Loading Curves," Journal of Materials Research, **11** (8), 1987–1995 (1996).

13. Underwood, J.H., "Residual-Stress Measurement Using Surface Displacements around an Indentation," EXPERIMENTAL MECHANICS, **13**, 373–380 (1973).

14. Olabi, A.G. and Hashmi, M.S.J., "Stress Relief Procedures for Low Carbon Steel (1020) Welded Components," Journal of Material Processing Technology, **56**, 552–562 (1996).